

Photon-induced desorption of larger species in UV-irradiated methane (CH₄) ice

H. Carrascosa,¹★ G.A. Cruz-Díaz,^{2,3} G. M. Muñoz Caro,¹† E. Dartois,⁴ Y. -J. Chen⁵‡

¹*Centro de Astrobiología (CSIC-INTA), Ctra. de Ajalvir, km 4, Torrejón de Ardoz, 28850 Madrid, Spain*

²*NASA Ames Research Center, Moffett Field, Mountain View, CA 94035, USA*

³*Bay Area Environmental Research Institute, Moffett Field, Mountain View, CA 94035, USA*

⁴*Institut des Sciences Moléculaires d'Orsay (ISMO), UMR8214, CNRS - Université de Paris-Sud, Université Paris-Saclay, Bât 520, Rue André R...*
91405 Orsay, France

⁵*Department of Physics, National Central University, Zhongli City, Taoyuan County 32054, Taiwan*

Accepted XXX. Received YYY; in original form ZZZ

ABSTRACT

At the low temperatures found in the interior of dense clouds and circumstellar regions, along with H₂O and smaller amounts of species such as CO, CO₂, or CH₃OH, the infrared features of CH₄ have been observed on icy dust grains. Ultraviolet (UV) photons induce different processes in ice mantles, affecting the molecular abundances detected in the gas-phase.

This work aims to understand the processes that occur in a pure CH₄ ice mantle submitted to UV irradiation. We studied photon-induced processes for the different photoproducts arising in the ice upon UV irradiation.

Experiments were carried out in ISAC, an ultra-high vacuum chamber equipped with a cryostat and an F-type UV-lamp reproducing the secondary UV-field induced by cosmic rays in dense clouds. Infrared spectroscopy and quadrupole mass spectrometry were used to monitor the solid and gas-phase, respectively, during the formation, irradiation, and warm-up of the ice.

Direct photodesorption of pure CH₄ was not observed. UV photons form CH_x· and H· radicals, leading to photoproducts such as H₂, C₂H₂, C₂H₆, and C₃H₈. Evidence for the photodesorption of C₂H₂ and photochemidesorption of C₂H₆ and C₃H₈ was found, the latter species is so far the largest molecule found to photochemidesorb. ¹³CH₄ experiments were also carried out to confirm the reliability of these results.

Key words: Methods: laboratory: molecular - ultraviolet: ISM - ISM: molecules - Astrochemistry

1 INTRODUCTION

The low temperatures present in dense interstellar clouds promote the formation of ice mantles around carbonaceous and silicate dust grains. In the outer regions of the cloud, the temperature and the UV field are too high for any molecule to freeze out. Deeper inside the cloud, there is sufficient screening from the external UV radiation field, and molecules form and accrete onto dust grains, thus forming ice mantles. Even the highly volatile species like CO and N₂ are frozen at 10 K. Methane has been detected in the interstellar medium (ISM) and dense clouds (Lacy et al. 1991;

Boogert et al. 1996; Öberg et al. 2008). Methane ice can be formed from successive hydrogenation of carbon atoms over a dust grain surface, from photoprocessing of CH₃OH ice, or even from gas-phase reactions and subsequent freeze out over dust grains (Öberg et al. 2008, and references therein). CH₄ constitutes a source of carbon atoms in ice mantles, with abundances around 5% and 2% of the water ice in low-mass and high-mass protostars, respectively (Dartois 2005; Öberg et al. 2011; Boogert et al. 2015). Complex organic molecules (COMs), containing six or more atoms and at least one carbon, can be formed from methane processing in the interstellar and circumstellar medium, or comets. These systems contain variable quantities, up to 4% relative to water, of solid methane, which is exposed to vacuum ultraviolet (UV) photons with a spectral energy distribution as simulated in our experiments (Gerakines

★ E-mail: hcarrascosa@cab.inta-csic.es

† E-mail: munozcg@cab.inta-csic.es

‡ E-mail: asperchen@phy.ncu.edu.tw

et al. 1996; Lin et al. 2014). In our Solar System, CH₄ has been detected on the surface of Triton (Cruikshank et al. 1993; Owen et al. 1993), Titan (McKay et al. 1997), and Pluto (Grundy et al. 2016), among others.

At the low temperatures that govern the interior of dense clouds, thermal energy is almost negligible, and ice processes driven by cosmic rays and UV photons play a significant role. Secondary UV radiation, generated by the interaction between cosmic rays and hydrogen molecules (Cecchi-Pestellini & Aiello 1992; Shen et al. 2004) is the main source of photons impinging on ice mantles in dense clouds. The absorption of UV photons by methane molecules in the ice leads to an efficient photochemistry. In this article, we explore the photon-induced desorption of molecules upon UV-irradiation of CH₄ in the laboratory.

The absorption of sufficient photon energy by a molecule on the ice surface counteracts the intermolecular forces with the surrounding species, allowing photon-induced desorption. UV photons, however, can also break covalent bonds, inducing the formation of radicals that may react to form new molecules, leading to photochemistry. Depending on the species present in the ice and the photon energy, UV radiation induces photon-induced desorption, photochemistry, or both.

The direct desorption of a molecule from the ice surface (van Hemert et al. 2015; Dupuy et al. 2017), after absorption of a photon, is of low efficiency compared to the indirect photodesorption, by which the photon is absorbed by another molecule and the photon energy is distributed to the surrounding molecules. In this case, a UV photon can be absorbed by a molecule in the subsurface layers of the ice, leading to electronic excitation. The energy from the relaxation to the ground state is redistributed to the neighboring molecules. A different kind of photon-induced desorption was observed when a surface molecule absorbs a photon and dissociates into photofragments that may recombine, forming a photoproduct. This photoproduct can desorb if the excess energy of the parent photofragments is sufficient to overcome the binding energy of the ice, due to the exothermicity of the reaction (Andersson & van Dishoeck 2008; Fayolle et al. 2013; Fillion et al. 2014; Bertin et al. 2016). Photochemical desorption or photochemidesorption only applies to species that are formed on the ice surface and are immediately ejected to the gas, leading to a constant photodesorption yield during the irradiation (Martín-Doménech et al. 2016, 2018; Cruz-Díaz et al. 2016).

The IR features arising from UV radiation or α -particle and proton bombardment of pure CH₄ ice were reported (Gerakines et al. 1996; Kaiser & Roessler 1998). More recently, Lin et al. (2014) and Lo et al. (2015) irradiated CH₄ ice at 3 K with monochromatic UV light from a synchrotron, and Dupuy et al. (2017) studied CH₄ photodesorption using monochromatic UV radiation. This work focuses on photon-induced desorption processes of CH₄ photoproducts using a continuum UV emission lamp that mimics the secondary UV-field in dense clouds. We will show that photoproducts desorb mainly via photochemides-

orption.

2 EXPERIMENTAL

Experiments were carried out in the InterStellar Astrochemistry Chamber (ISAC) located at the Centro de Astrobiología (for a detailed description of ISAC see Muñoz Caro et al. (2010)). ISAC is an ultra-high vacuum chamber with a base pressure around 4×10^{-11} mbar, similar to the pressure in dense interstellar clouds. A closed-cycle helium cryostat allows to cool down to 8 K, a temperature similar to that of dust grains in the inner parts of dense interstellar clouds. CH₄ (gas, Praxair 99.95%) and ¹³CH₄ (gas, Cambridge Isotopes Laboratories 99.9%) were used for the experiments. Gases at a pressure of 2×10^{-7} mbar were introduced in the UHV-chamber through a stainless steel tube at normal incidence angle with respect to the MgF₂ substrate. The low temperature of the substrate led to the formation of amorphous ices (Hudson et al. 2015). The column density of the ice samples corresponds to an absorption of about 90% of the incident photon flux in the deposited ice layers. To estimate the number of UV photons absorbed, we adopted the UV absorption cross-section of CH₄ ice measured by Cruz-Díaz et al. (2014).

Fourier-Transform Infrared Spectroscopy (FTIR) measured with a Bruker Vertex 70 spectrometer equipped with a deuterated triglycine sulfate detector (DTGS) was used to monitor the column densities and composition of the ice samples. IR spectra were measured with a resolution of 2 cm⁻¹ after deposition of the ice, after each irradiation step, and also during the warm-up. The measured spectral range in the reported experiments spans from 6000 to 1200 cm⁻¹ (1.66 to 8.33 μ m), since the MgF₂ substrate becomes optically thick at longer wavelengths. The column density of the ice layer was determined using equation 1, where N is the column density of the molecule of interest in molec · cm⁻², A is the band strength of the considered band in cm · molecule⁻¹, τ_v the optical depth of the band, and dv the wavenumber differential in cm⁻¹:

$$N = \frac{1}{A} \int_{band} \tau_v dv. \quad (1)$$

Ice samples were irradiated using an F-type microwave discharge hydrogen lamp (MDHL) from Ophos Instruments, providing an UV flux of 2×10^{14} photons · cm⁻² · s⁻¹ and 8.6 eV average photon energy (e. g. Cruz-Díaz et al. (2016)). The MgF₂ window between the MDHL and the vacuum chamber leads to a cut-off at 114 nm (10.87 eV). Destruction cross-section of CH₄, and similarly of ¹³CH₄, were obtained using equation 2, where $N_t(\text{CH}_4)$ and $N_0(\text{CH}_4)$ are the column densities measured by FTIR before and after the irradiation, respectively, in molec · cm⁻², ϕ is the UV flux in photons · cm⁻² · s⁻¹, t is the irradiation time in s, which belongs to the first irradiation period, as the ice is less processed at the beginning, and $\sigma_{des}(\text{CH}_4)$ is

the destruction cross-section in cm².

$$N_t(\text{CH}_4) = N_0(\text{CH}_4) \times e^{-\phi t \sigma_{\text{des}}(\text{CH}_4)} \quad (2)$$

Formation cross-section for ethane molecules ($\sigma_{\text{for}}(\text{C}_2\text{H}_6)$) was obtained using equation 3, where $\frac{dN(\text{C}_2\text{H}_6)}{dt}$ is the variation of the column density of ethane molecules after irradiation time, t is the irradiation time in s, and $N(\text{CH}_4)$ is the average column density of methane during the irradiation interval.

$$\frac{dN(\text{C}_2\text{H}_6)}{dt} = -\phi \times t \times N(\text{CH}_4) \times \sigma_{\text{for}}(\text{C}_2\text{H}_6) \quad (3)$$

The gas-phase was monitored during deposition, irradiation, and warm-up processes using a Pfeiffer Prisma quadrupole mass spectrometer (QMS) equipped with a Channeltron detector. Molecules were ionized by electron impact of 70 eV and accelerated into the mass filter of the QMS, leading to a characteristic fragmentation pattern for each species. From the ion current obtained in the QMS for each molecular fragment, a quantification of the gas-phase molecules was done following the procedure presented in Martín-Doménech et al. (2015). After baseline and blank (no ice sample) irradiation corrections, the area below the QMS during each irradiation period was calculated, obtaining the ion current as a function of the photon dose. Applying Eq. 4 and the values in Table 1, photodesorption rates of methane, ethane and propane were obtained by monitoring $\frac{m}{z} = 15$, $\frac{m}{z} = 30$, and $\frac{m}{z} = 43$, respectively. These $\frac{m}{z}$ fragments were selected considering the possible contribution of other molecules and the relative intensity for each of the fragments. In Eq. 4, $N(\text{mol})$ is the photodesorption rate in molec · photon⁻¹, $A\left(\frac{m}{z}\right)$ is the area obtained from the QMS normalized by the number of incident photons, k_{CO} is the proportionality constant from the calibration of the QMS in a CO ice irradiation experiment (see Martín-Doménech et al. (2015)), $\sigma^+(\text{mol})$ is the ionization cross-section of each species ionized at a voltage of 70 eV in the QMS (data adopted from the National Institute of Standards and Technology), $IF(z)$ is the ionization factor, which has been considered unity for all molecules, as most of them will be charged once, FF is the fragmentation factor, it refers to the percentage of molecules which account for a given $\left(\frac{m}{z}\right)$ value (using the mass spectrum of methane measured by our QMS during deposition, while the mass spectra from NIST database was used for the photoproducts), and $S\left(\frac{m}{z}\right)$ is the sensitivity of the QMS, which depends on the ion current generated at the QMS as a function of the mass of each molecule (for calculation details, see Martín-Doménech et al. (2015)).

$$N(\text{mol}) = \frac{A\left(\frac{m}{z}\right)}{k_{\text{CO}}} \cdot \frac{\sigma^+(\text{CO})}{\sigma^+(\text{mol})} \cdot \frac{IF(\text{CO}^+)}{IF(z)} \cdot \frac{FF(28)}{FF(m)} \cdot \frac{S(28)}{S\left(\frac{m}{z}\right)} \quad (4)$$

Table 1. Values adopted for the calculation of photodesorption rates by QMS

Parameter	CO	CH ₄	C ₂ H ₆	C ₃ H ₈
$k_{\text{CO}} \left(\frac{\text{A} \cdot \text{min}}{\text{molecule}} \right)$	$1.32 \cdot 10^5$	-	-	-
$\sigma^+(\text{mol}) \text{ (A}^2\text{)}$	2.516	3.524	6.422	8.619
FF	0.939	0.419	0.122*	0.0757*

* Values taken from the National Institute of Standards and Technology (NIST) database.

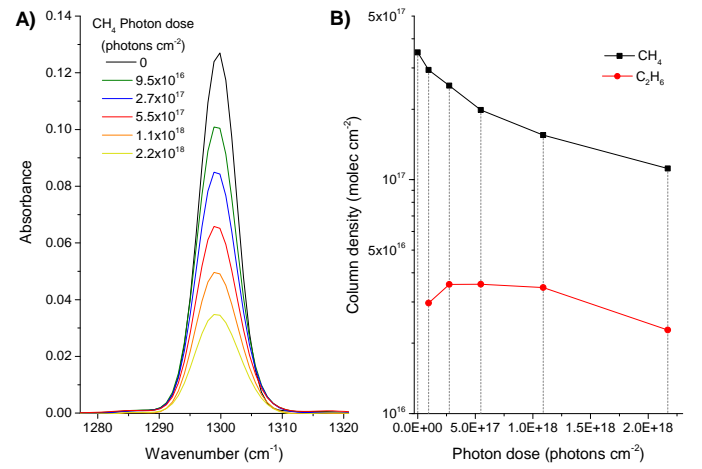


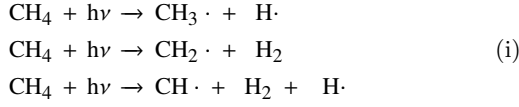
Figure 1. A) Evolution of the ν_3 vibration mode of methane as a function of the photon dose for CH₄. B) Column density calculated for CH₄ and C₂H₆ after each irradiation period.

After the irradiation steps, ice samples were warmed up until room temperature using a LakeShore Model 331 temperature controller. The temperature was monitored by a silicon diode sensor with a sensitivity of 0.1 K, located underneath the sample holder.

3 RESULTS AND DISCUSSION

3.1 Photochemical processes

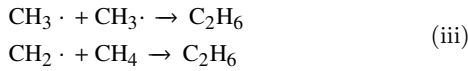
Fig. 1A shows the evolution of the ν_3 stretching mode of CH₄ (1301 cm⁻¹). The reaction network presented in scheme i shows that UV photons can dissociate methane molecules producing CH₃· and H· radicals, CH₂· radicals and H₂ molecules or, to a lesser extent, CH· radicals, H₂ and H· radicals. The position of the ν_3 IR band does not change, while its intensity is reduced. In the gas-phase, for 123.6 nm (10.03 eV) photons, the quantum yields for the second and third reactions are 0.5 and 0.06, respectively (Okabe 1978).



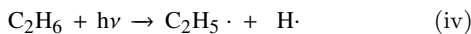
Radicals produced from methane dissociation will recombine giving rise to new species. This observation is supported by the formation of hydrogenated amorphous carbon (a-C:H) at 10 K in similar CH₄ irradiation experiments (Dartois et al. 2005). As a consequence, bands related to CH_x· radicals were not detected in IR spectra (e. g. the 3150 cm⁻¹ band for CH₃·, de Barros et al. (2011)). H· radicals can diffuse inside the ice and recombine producing H₂ molecules, as shown in Scheme ii.



The reaction of two CH₃· radicals in the gas-phase produces ethane, C₂H₆, (Scheme iii), with a rate constant of $5 \times 10^{-11} \text{ cm}^3 \text{ molec}^{-1} \text{ s}^{-1}$ (Okabe 1978), leading to the appearance of its characteristic IR bands (see Fig. 2 and Table. 2). Ethane can also be produced from the reaction between a CH₂· radical and a CH₄ molecule, although the lower formation rate of CH₂· radicals would probably determine a minor production rate by this route.



As shown in Fig. 2, bands related to C-H stretching modes from different molecules appeared in the IR spectrum between 3000-2800 cm⁻¹ upon irradiation. The profile of this region was fitted using 10 Gaussian curves. The bands assignment is shown in Table 2 for CH₄ and ¹³CH₄ irradiations. Within the first steps of irradiation, the integrated IR absorption of the photoproducts increases as a consequence of the ice processing. However, IR bands related to ethane (2975, 2941 and 2883 cm⁻¹) decrease for longer irradiation times, while other IR bands are still growing. The formation of hydrogen molecules, which can escape from the ice, determines that the proportion of carbon to hydrogen increases during the irradiation, and CH₃· radicals are more and more scarce. Therefore, the production of C₂H₆ (Scheme iii) molecules is lowered, whereas its dissociation (Scheme iv) does not change, in agreement with the observed ethane band intensities.



The CH₄ band at 1301 cm⁻¹ was selected for quantification of its column density using Eq. 1 and assuming a band strength of $6.1 \times 10^{-18} \text{ cm} \cdot \text{molec}^{-1}$ (Gerakines et al. 1996; Kaiser & Roessler 1998). Fig. 1B shows the column density of methane and ethane as a function of the

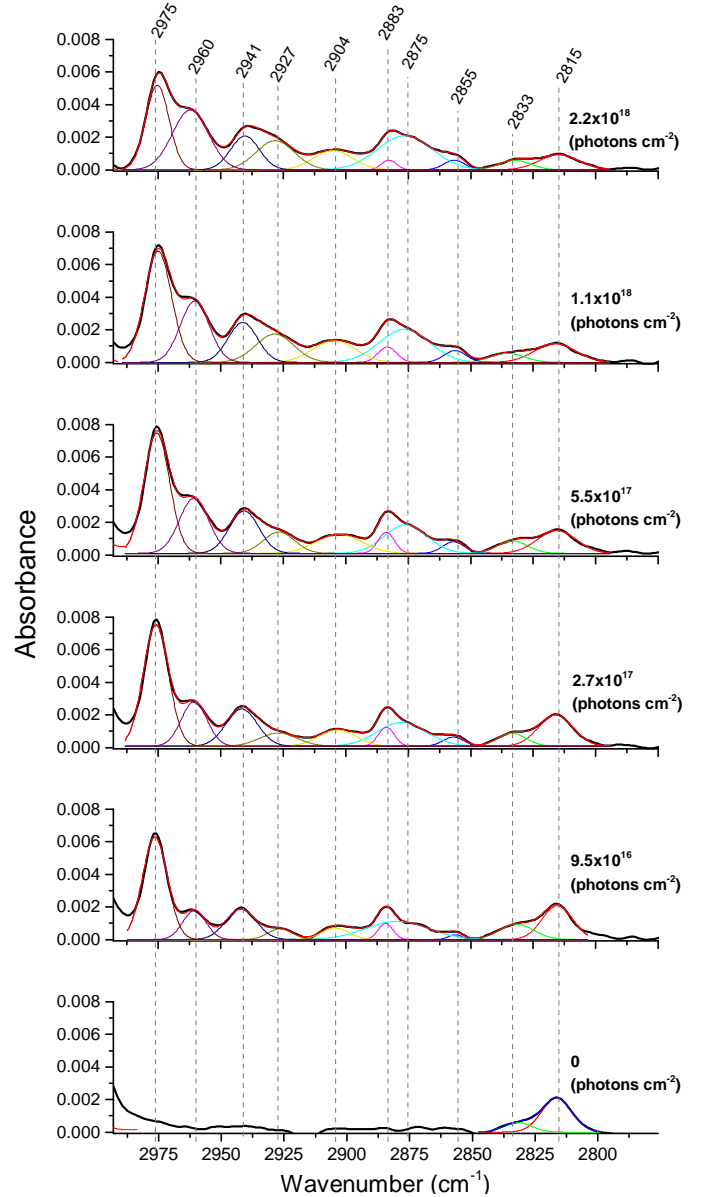


Figure 2. Evolution of CH₄ IR features between 3000-2800 cm⁻¹ under UV irradiation. Black trace belongs to the original spectra. Red trace represents the sum of 10 Gaussian profiles. Gaussian profiles were used to take peak positions and calculate the abundances.

incident photon flux. The Gaussian profile at 2975 cm⁻¹ was used to obtain the column density of C₂H₆ molecules, using a band strength of $1.3 \times 10^{17} \text{ cm} \cdot \text{molec}^{-1}$, following Gerakines et al. (1996). Taking into account the destruction cross-section of methane shown in Table 3, and the column density of ethane molecules after the first irradiation step, the formation cross-sections of C₂H₆ was obtained using equation 3 (see Table 3). Ethane was found to be the main molecular photoproduct for short irradiation periods, but, as the amount of CH₃· radicals is reduced, less hydrogenated compounds arise in the ice upon further irradiation.

Dissociation of ethane molecules gives rise to the forma-

Table 2. Main IR features detected between 3100-2800 cm⁻¹ after 240 min irradiation of a pure CH₄ ice (left) and a pure ¹³CH₄ ice (right). Positions belong to the centre of the Gaussian profiles, shown in Fig. 2 for a CH₄ experiment. ¹³CH₄ IR spectra (not shown) revealed a similar profile.

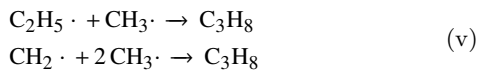
CH ₄			¹³ CH ₄		
Frequency (cm ⁻¹)	Assignment	Reference	Frequency (cm ⁻¹)	Assignment	Reference
3009	CH ₄	1, 6	3000	¹³ CH ₄	7
2975	C ₂ H ₆	1, 2, 8	2966	¹³ C ₂ H ₆	7
2960	R-CH ₂ -R'	2, 3, 9	2958	R- ¹³ CH ₃	7
2941	C ₂ H ₆	2	2940	¹³ C ₂ H ₆	This work
2927	R-CH ₂ -R'	4	2931	R- ¹³ CH ₂ -R	7
2904	?		2909	?	
2883	C ₂ H ₆	1, 2, 3, 5, 8	2879	R,R'- ¹³ CH-R'' / ¹³ C ₂ H ₆	7
2875	R-CH ₃	5	2871	R- ¹³ CH ₃	This work
2855	R-CH ₂ -R'	2	2843	R- ¹³ CH ₂ -R'	This work
2833	R-CH ₃	5	2817	R- ¹³ CH ₃	This work
2815	CH ₄	1, 7	2807	¹³ CH ₄	This work

1- Gerakines et al. (1996); 2- de Barros et al. (2011); 3- Moore & Hudson (2003); 4- Dartois et al. (2005); 5- Bennett et al. (2006); 6- d'Hendecourt et al. (1986); 7- Kaiser & Roessler (1998); 8- Lin et al. (2014); 9- Baratta et al. (2002)

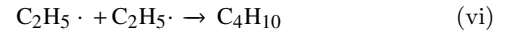
Table 3. Column density and destruction/formation cross-section (σ) of methane and ethane for CH₄ ice samples. A 10% error was estimated by the sum of the errors from the column density, and the MDHL, photomultiplier and ammeter stabilities for the incident cross-sections, whereas in the absorption cross-section presented in Cruz-Diaz et al. (2014), a 20% error is assumed for the absorbed cross-sections.

N _{t=0} (molec·cm ⁻²)	photon flux (ϕ)	Species	σ (cm ²)
3.5×10 ¹⁷	incident	CH ₄	1.9 ×10 ⁻¹⁸
		C ₂ H ₆	1.0 ×10 ⁻¹⁸
3.5×10 ¹⁷	absorbed	CH ₄	2.2 ×10 ⁻¹⁸
		C ₂ H ₆	1.2 ×10 ⁻¹⁸

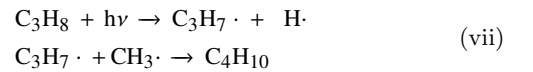
tion of other photoproducts. C₂H₅· radicals produced from ethane dissociation may react with CH₃· radicals, thus forming propane (Scheme v). Propane can also be produced from the reaction of a CH₂· radical with two CH₃· radicals. However, the probability of three species reacting simultaneously should be lower in the solid phase, and this reaction pathway may be negligible. The column density of propane molecules was not possible to determine, as its IR bands (e. g. 2960 cm⁻¹) overlap with vibration modes from a-C:H. The proposed reaction pathway for the formation of propane is provided below:



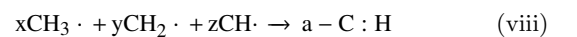
Ethyl radicals produced from methane dissociation may also react, forming butane molecules.



C₄H₁₀ can also be produced from the rupture of propane molecules and the subsequent reaction with a methyl radical (Scheme vii). However, as propane was found to be less abundant, this reaction is not expected to be influential in our experiments. Hence no butane was detected among the photoproducts in our experiments.



We mentioned that chemical reactions between radicals formed by CH₄ ice irradiation lead to a complex branched network of C and H atoms, known as hydrogenated amorphous carbon, a-C:H (Dartois et al. 2005). The refractory a-C:H is the main constituent of carbonaceous dust grains observed in the ISM (Dartois et al. 2005). Subsequent irradiation leads to a reduction of C-H bonds in a-C:H, the C to H rate changes during the irradiation, and a less hydrogenated amorphous carbon is obtained.



3.2 Vacuum UV spectra

Fig. 3 shows the VUV spectrum of methane ice. CH₄ has a strong absorption from the cut-off of the lamp

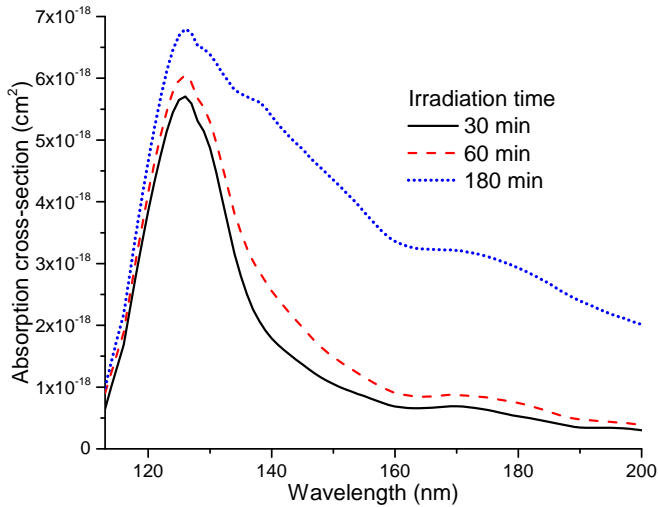


Figure 3. VUV absorption spectra of CH₄ ice. The bump appearing at 170 nm could be due to the presence of C₂H₄ molecules, see text.

(114 nm, 10.87 eV) to 133 nm (9.32 eV), and almost no absorption above 140 nm (8.86 eV) (Wu et al. 2012; Cruz-Diaz et al. 2014). During the irradiation steps, the formation of different photoproducts involving C-C bonds is responsible for the extended UV absorbance up to 180 nm (6.89 eV). These include C₂H₆, C₃H₈, the a-C:H residue, and probably C₂H₂ identified as a photodesorbing species in Sect. 3.3. C₂H₄, which was not identified by IR or QMS, could be responsible for the bump appearing between 160-180 nm (7.75-6.89 eV), according to its UV absorption spectrum (Lu et al. 2004; Young et al. 2018).

3.3 Photon-induced desorption

The QMS monitored the desorption of molecules from the ice sample. The time-dependent ion current from each molecular fragment served to detect the evolution of molecules in the gas-phase (see Sect. 2). Fig. 4A, B, and C represent the ion current measured during the irradiation of pure CH₄ ice for the main $\frac{m}{z}$ fragments from H₂, C₂H₆, and C₃H₈, respectively.

H· radicals produced from methane dissociation can diffuse through the ice even at 8 K, thus forming hydrogen molecules that can escape from the ice to the gas-phase, allowing their detection by QMS for short irradiation times. The presence of H₂ background contamination intrinsic to UHV chambers and its possible release from turbomolecular pumps prevented the quantification of H₂ photodesorption. Additionally, the ion current generated by H₂ in the QMS is reduced for longer irradiation times as the column density of CH₄ ice diminishes.

Dupuy et al. (2017) reported CH₄ photodesorption from pure CH₄ ice for monochromatic photon energies above 9 eV, where the UV absorption of CH₄ becomes important (Cruz-Diaz et al. 2014). They found photodes-

orption of methane to be around 2.3×10^{-3} molecules per photon at Ly- α photon energy, and 2.2×10^{-3} molecules per photon integrating over the Gredel et al. (1989) photon distribution. However, CH₄ was not found to photodesorb in our experiments using the continuum emission MDHL, with a calculated upper limit of 1.7×10^{-4} molecules per incident photon. This difference could be explained by the onset of CH₄ photodesorption starting at energies of about 9.2 eV (135 nm), with a large absorption cross-section of solid methane at Ly- α , and even higher above 11 eV (Wu et al. 2012), while there is almost no UV-absorption corresponding to the MDHL molecular emission range below 9.2 eV, i. e. a lower average absorption cross-section over the photon energy range covered by the MDHL, see Cruz-Diaz et al. (2014). Besides, when UV photons dissociate CH₄ ice molecules, H· atoms escape from the solid phase, leaving CH₃· radicals behind. Therefore, the backward reaction to produce CH₄ is inhibited, in particular at the surface of the ice, which may explain the absence of CH₄ photochemidesorption in our experiments with pure CH₄ ice. Cruz-Diaz et al. (2016) found that UV irradiation of pure CH₃OH ice gives rise to CH₃· and HCO species, among others. A likely explanation is that in Cruz-Diaz et al. (2016) experiments, CH₃· radicals react with HCO· and other species, allowing the formation of CH₄ molecules and their subsequent photochemidesorption when these reactions occur at the surface.

NH· and NH₂· radicals produced from UV irradiation of pure NH₃ ice were found to react mainly at temperatures well above 10 K (Martín-Doménech et al. 2018). Thus, the photoprocessing of the ice is limited to the production of radicals, and other photoproducts appear mainly during the warm-up phase. On the contrary, our experiments showed that radicals produced from UV irradiation of CH₄ are more reactive at low temperature, in agreement with other works (e. g. Lin et al. 2014).

CH₃· radicals produced from CH₄ dissociation react in the ice, leading to an efficient ethane formation at the ice bulk and surface. QMS detected photon-induced desorption of the so-formed ethane molecules. The energy released during the formation of ethane from two methyl radicals overcomes the intermolecular interactions of the new molecule with the ice, which therefore photochemidesorbs as soon as it is formed (with a rate of 8×10^{-4} molecules per incident photon¹). A similar effect is observed for propane, which is, to our knowledge, the largest molecule found to photochemidesorb, with a rate of 2.4×10^{-3} molecules per incident photon. The constant QMS ion current measured for ethane and propane molecules supports a photochemidesorption mechanism (Cruz-Diaz et al. 2016; Martín-Doménech et al. 2015, 2016). The surface of the ice is renewed upon UV-irradiation due to formation of photoproducts and their eventual desorption if these species are formed at the ice surface. Radical formation and recombination also occurs in the ice bulk and become

¹ Values of the photon-induced desorption yields can vary by a factor of 2, estimated by the errors in the parameters in Eq. 4, see Martín-Doménech et al. (2016)

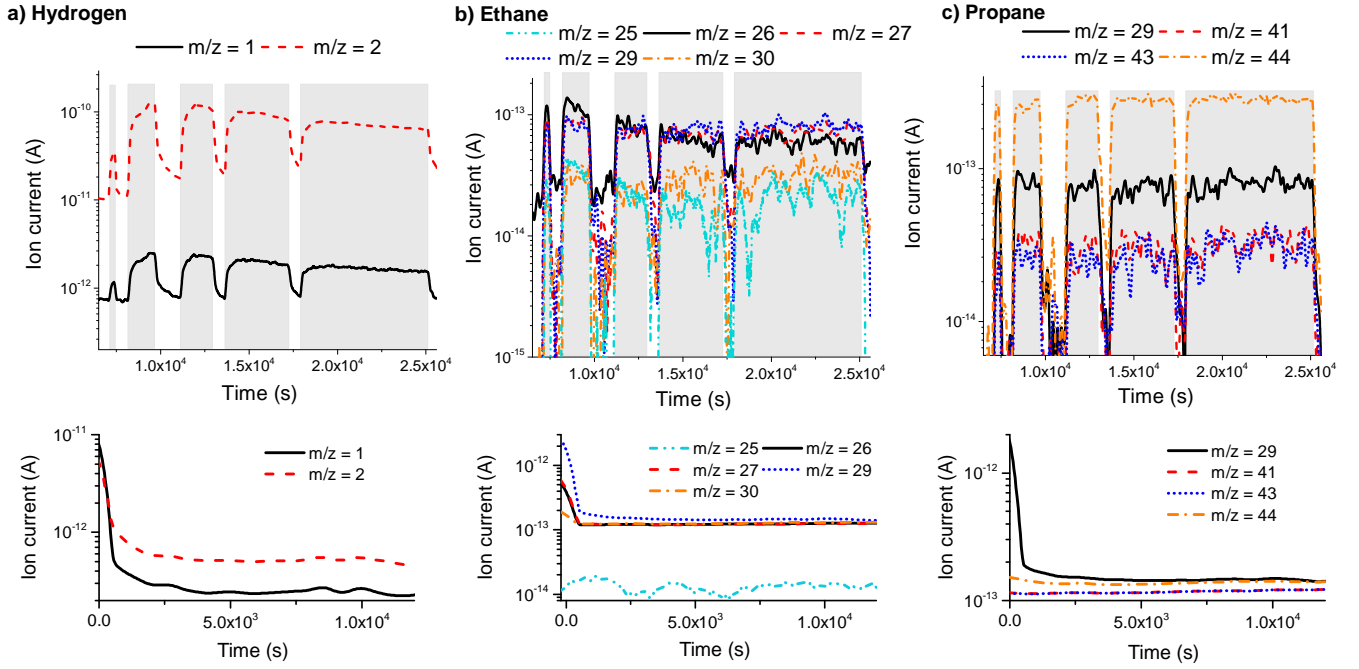


Figure 4. Top: photodesorption of the three main photoproducts formed from UV-irradiation of CH₄, H₂, C₂H₆ and C₃H₈. Gray areas represent the time lapse when the lamp is turned on. Bottom: same $\frac{m}{z}$ fragments from a blank experiment where CH₄ ice was not irradiated. Note that the Y-axis is in a logarithmic scale.

gradually exposed at the renewed surface due to desorption of the top monolayers during irradiation. The surface is thus enriched in ethane and propane molecules. The constant desorption rates of these species during irradiation indicates that only when they are formed directly on the surface, they can escape from the ice. Indeed, an ethane/propane molecule formed in the bulk that becomes later exposed to the surface will photodissociate rather than desorb when it absorbs a UV-photon.

Interestingly, Fig. 4B shows that $\frac{m}{z} = 25$, and 26, decrease over the irradiation steps, while $\frac{m}{z} = 27$, 28, 29, and 30 remain constant, suggesting that a second contribution is present within $\frac{m}{z} = 25$, and 26. C₂H₂ photodesorption may be responsible for this behaviour, since $\frac{m}{z} = 26$ is the most intense molecular fragment of acetylene, followed by $\frac{m}{z} = 25$, and almost no $\frac{m}{z} = 24$ is produced. Acetylene can be produced from dehydrogenation of ethane molecules, although ethane photochemidesorption would inhibit acetylene formation in the surface, and therefore its photodesorption. C₂H₂ can also be formed from the reaction between two CH₃· radicals produced directly from CH₄ dissociation, as shown in Scheme ix. Okabe (1978) reports a yield value of 0.06 with respect to the production of CH₃· radicals for the gas-phase using Ly- α photons. Recently, Lin et al. (2014) measured the threshold energy of this reaction in CH₄ ice at 3 K, obtaining a value of 9.2 eV (134.8 nm). Therefore, the continuum emission of our MDHL may favour this reaction.



Table 4. Binding energy, in K, of desorbing species during the warm-up of the samples.

Species	T _{des} (K)	E _b (K)	Species	T _{des} (K)	E _b (K)
CH ₄	38.6	1193	¹³ CH ₄	38.7	1196
C ₂ H ₆	66.1	2042	¹³ C ₂ H ₆	67.0	2070
C ₃ H ₈	83.5	2580	¹³ C ₃ H ₈	85.0	2626

3.4 Thermal desorption

After irradiation, CH₄ ice samples were warmed up at a rate of 1 K/min. IR spectra were collected during the temperature programmed desorption (TPD). Methane bands at 3009, 2815 and 1300 cm⁻¹ disappear at a temperature lower than 40 K, while photoproducts (mainly ethane, propane and hydrogenated amorphous carbon), will remain in the ice at higher temperatures. Fig. 5 shows the IR spectra measured during the TPD at different temperatures. Bands identified with ethane (2975, 2941 and 2883 cm⁻¹) disappear gradually as the temperature increases, and they are not observed above 70 K. Meanwhile, IR bands at 2960 cm⁻¹, 2926 cm⁻¹, 2870 cm⁻¹ and 2857 cm⁻¹, related to different stretching modes of a-C:H (Dartois et al. 2005), are still clearly observable at 300 K.

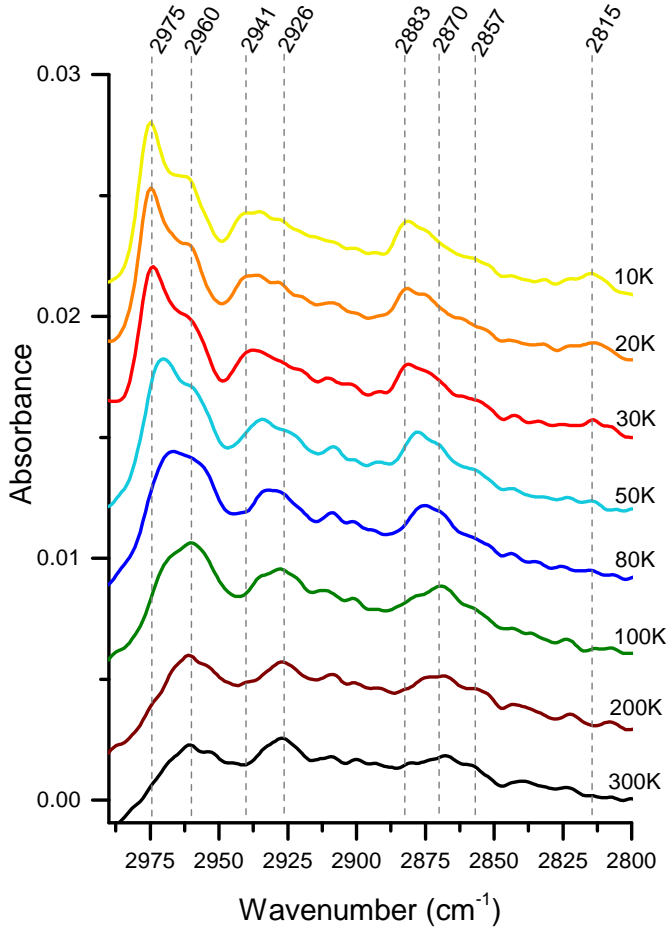


Figure 5. IR spectra collected during warm-up of irradiated CH₄ ice at different temperatures. Spectra were offset for clarity.

The ion current of different $\frac{m}{z}$ fragments during the TPD process is represented in Fig. 6. CH₄ molecules (Fig. 6A) desorb thermally from the irradiated CH₄ ice at 38.6 K. A second peak that appears near 66.5 K is related to the thermal desorption of methane ice that accreted outside the sample substrate in cold areas of the cold finger. Indeed, this peak disappears if the cold finger of the cryostat is warmed up at the same rate with the thermal resistance and the cryostat off (*natural* TPD). The thermal desorption of C₂H₆ occurs at 66.1 K. Two clear peaks are also observed in Fig. 6B. The one at 38.6 K represents the ethane molecules co-desorbing with CH₄, with $\frac{m}{z} = 30$ for the molecular ion, C₂H₆⁺, and other fragments at $\frac{m}{z} = 29, 28, 27, 26$ and 25 with relative intensities similar to those in the NIST database for ethane. As CH₄ is the primary molecule present in the ice, its thermal desorption can drag other molecules. But other ethane molecules will remain in the ice until 66.1 K, where C₂H₆ molecules desorb from pure ethane ice (in agreement with Hudson et al. (2009)). Propane co-desorption with methane and ethane molecules is observed at 38.6 K and 66.1 K, respectively. The third peak, appearing at 83.5 K, belongs to the propane ice thermal desorption. Following Luna et al. (2017), the binding energies of these species are obtained multiplying the peak temperatures by a factor of 30.9. These values for CH₄,

C₂H₆ and C₃H₈ and their homologous ¹³C isotopologues are shown in Table 4.

To further confirm the results obtained for CH₄ ice, experiments were repeated using ¹³CH₄. The ion current of different $\frac{m}{z}$ fragments is represented in Fig. 6 (bottom part) for a TPD from a ¹³CH₄ ice sample. ¹³CH₄ desorbs thermally at 38.7 K. ¹³C₂H₆ co-desorbs with methane, while its pure thermal desorption occurs at 67.0 K. Both processes are similar to the ones found for the CH₄ ice. Propane co-desorption with CH₄ and C₂H₆ at 38.6 K and 66.1 K in the CH₄ experiment, monitored by $\frac{m}{z} = 43$ and 44, were not confirmed by their corresponding fragments $\frac{m}{z} = 46$ and 47 in the ¹³CH₄ experiment. While $\frac{m}{z} = 44$ could suffer from CO₂ contamination, the $\frac{m}{z} = 43$ desorption could not be identified with a contaminant. Nevertheless, the desorption of C₃H₈ at 83.5 K was reproduced in the ¹³CH₄ experiment as a peak appearing at 85.0 K (Fig. 6F). Thermal desorption of ¹³CH₄, ¹³C₂H₆ and ¹³C₃H₈ takes place at slightly higher temperatures when compared to the homologous species with ¹²C, as a consequence of their larger molecular mass.

In this work, ¹³CH₄ was only employed to rule out any potential source of carbon contamination. Some processes were not quantified, such as propane formation or photochemidesorption of species in the ¹³CH₄ experiment. Despite this, similar trends regarding photochemistry and photodesorption were obtained.

4 ASTROPHYSICAL IMPLICATIONS

In the interior of dense clouds, the dust temperature is too low to induce thermal processes, and the interstellar radiation UV field cannot penetrate deep into the cloud. Therefore, secondary UV-photons drive the photolytic processes in these regions (see Sect. 1). This work reports measurements of the UV photon-induced processes over a pure CH₄ ice, as a first approximation to a more realistic scenario, in line with previous works that addressed the photon-induced behaviour of pure ice components. Since CH₄ is thought to be mainly formed from successive hydrogenation of C atoms (Öberg et al. 2008), methane might be present in a H₂O-rich environment. Intermolecular forces binding CH₄ molecules in the ice will obviously depend on the ice mantle composition and this will also affect strongly its photodesorption and photochemistry. For instance, contrary to the case of pure CH₄ ice, reported in this paper, CH₄ formed by methanol or ethanol ice irradiation is found to photochemidesorb (Cruz-Díaz et al. 2016; Martín-Doménech et al. 2016).

Boogert et al. (1996); d’Hendecourt et al. (1996) reported methane abundance in dense interstellar clouds up to 1.9% relative to water. In addition, d’Hendecourt et al. (1996) estimated a column density of 4.3×10^{17} cm⁻² toward RAFGL 7009S, a circumstellar environment, representing a 4% abundance relative to water ice. Öberg et al. (2008) analyzed CH₄ abundances toward different low-mass young stellar objects, finding an average value

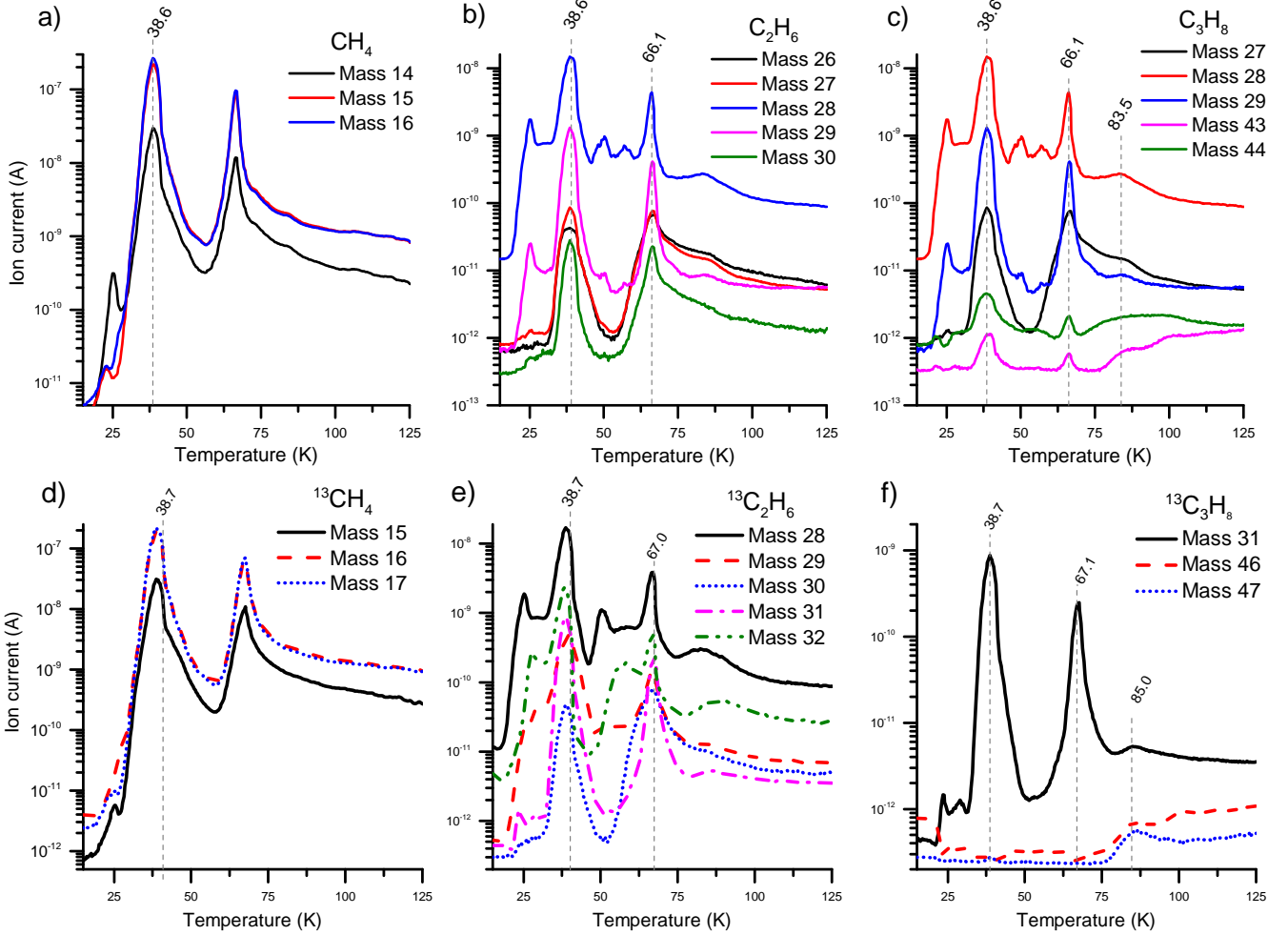


Figure 6. TPD curves for the main species present in the ice after the irradiation period for pure CH_4 ice (top) and for pure $^{13}\text{CH}_4$ ice (bottom). Note that the Y-axis is in a logarithmic scale.

of 5.8% abundance relative to water. CH_4 is expected to play a role in the production of COMs in the ISM. From pure CH_4 ice irradiation, larger molecules are formed, and eventually ejected to the gas-phase, such as ethane and propane. Complementary experiments are required to gain a better understanding of the behaviour of CH_4 in different ice mixtures, such as $\text{H}_2\text{O}:\text{CH}_4$ (Martín-Doménech et al. 2016) or $\text{CO}:\text{CH}_4$ mixtures. In the $\text{H}_2\text{O}:\text{CH}_4$ ice irradiation, Martín-Doménech et al. (2016) observed the photon-induced desorption of formaldehyde. Öberg et al. (2010) found that the destruction cross-section of CH_4 molecules is increased in a water-rich environment.

Photochemidesorption of C_2H_6 was found to be about 8×10^{-4} molecules per incident photon, while that of C_3H_8 is 2.4×10^{-3} molecules per incident photon. As pure CH_4 ice may not be present within interstellar conditions, these values can be taken as upper limits to explain the gas-phase abundance of ethane and propane molecules. On the other hand, pure CH_4 is abundant in transneptunian objects (TNOs) such as Triton or Pluto (Owen et al. 1993, and references therein) and may be a common ice component in outer regions of protoplanetary disks. The

composition of Pluto's atmosphere contains not only N_2 and CH_4 , but also C_2H_2 , C_2H_4 , and C_2H_6 (Young et al. 2018). The surface temperature is high enough to allow thermal desorption of CH_4 , explaining its presence in the gas-phase, while other species require the presence of alternative pathways. Our experiments show that photon-induced processes, as discussed in Wong et al. (2017), can contribute to the processes enriching the gas-phase abundance of C_2H_6 and C_2H_2 species, while C_2H_4 was not detected in the gas-phase. These results qualitatively agree with Pluto observations reported by Young et al. (2018), which measured C_2H_6 to be the most abundant hydrocarbon (apart from CH_4), followed by C_2H_2 and C_2H_4 .

Our results can also be extended to the discussion of the evolution of carbon-enriched comets, which contain relatively large abundances of methane molecules, up to 1% relative to water (Mumma & Charnley 2011). In these objects, photolysis of CH_4 gives rise to ethane and acetylene molecules, with cometary abundances ranging from 0.1-2% and 0.09-0.5%, respectively, which were also detected in our experiments. A full study of the evolution with more real-

istic CH₄/H₂O cometary ice analog mixtures is required to better constrain the photochemistry in these objects.

5 CONCLUSIONS

Lin et al. (2014) and Lo et al. (2015) irradiated CH₄ samples, both pure and dispersed in a neon matrix, at 3 K, with monochromatic UV photons at wavelengths ranging from Ly- α to 190 nm. In addition to other photoproducts, they reported the formation of C₂H₆, C₂H₄ and C₂H₂ molecules as well as CH₃· and CH· radicals. They found CH_x· radicals to react even at 3 K in a CH₄:Ne = 1:10.000 matrix. In our experiments, CH_x· radicals were not detected, as their lifetime is not high enough at 8 K. Their irradiation experiments at Ly- α wavelengths showed similar abundances to our experiments, C₂H₆ being the most abundant photoproduct, followed by C₂H₂ and C₂H₄. However, since the abundances depend on the wavelength used for irradiation, a different emission spectrum may change the photon-induced desorption processes found in our experiments.

In addition to the monochromatic irradiation of methane samples, Bossa et al. (2015) used a continuum emission hydrogen lamp, similar to our experiments. They deposited samples at 20 K, thus having a phase II methane instead of an amorphous one (Hudson et al. 2015). They reported the formation of ethane, ethylene and acetylene, but, as in our experiments, radical species were not detected.

Similar photoproducts were found by Abplanalp et al. (2018), who irradiated methane ices at 5.5 K with keV electrons, monochromatic Ly- α photons and continuum emission photons (from 112.7-169.8 nm, or 11.0-7.3 eV) using a deuterium lamp. They reported the presence of radical species and small hydrocarbons measured in the ice by infrared spectroscopy. Additionally, they reported the detection of larger hydrocarbon chains and cyclic species during the warm-up of the samples by time-of-flight mass spectrometry analysis.

Baratta et al. (2002) reported experiments of a pure CH₄ ice irradiated by 30 keV He⁺ ions and UV photons. They measured the column density of methane, ethane and propane after different irradiation doses. de Barros et al. (2011) compared the effects of pure CH₄ ice processing using different irradiation sources: oxygen MeV ions, protons, α -particles and electrons. In this work, we have provided experiments regarding UV-irradiation (from 7.6 eV to 10.8 eV) of pure CH₄ ice aiming to study the photon-induced desorption of photoproducts. Ethane molecules were found to account for 54% of the dissociated methane molecules at the beginning of the irradiation. Other photoproducts, such as C₃H₈ and the progressive formation of a-C:H, account for the rest of C atoms from methane dissociation, although the proportions varied during the irradiation. Propane was not quantified, as its main bands overlap with those of a-C:H, which is formed from the beginning of the irradiation, in agreement with Dartois et al. (2005).

Gerakines et al. (1996) measured the photolysis and

formation cross-section of CH₄ and C₂H₆, respectively. They found σ_{des} of methane to be 7.2×10^{-19} cm², while our experiments showed a value of 2.2×10^{-18} cm². The following reasons could explain our higher σ_{des} . First, Gerakines et al. (1996) calculated their value as a function of the incident photon dose, while we took into account the absorption from the ice, thus removing the contribution of low energy UV-photons which are not absorbed by the CH₄ ice sample. Additionally, the total flux was estimated in our experiments by in-situ measurements with a Ni-mesh (see González Díaz et al. (2019)) whereas Gerakines et al. (1996) assumed a constant mean flux of 10^{15} photons cm⁻² s⁻¹. Finally, the poorer vacuum conditions in Gerakines et al. (1996) setup could contribute to reduce the photodissociation of CH₄ due to background water accretion. σ_{for} of ethane found in our experiments (1.2×10^{-18} cm²) is also larger than the one they reported (3.2×10^{-19} cm²).

Photodesorption mechanisms were studied for CH₄ and its daughter molecules. Dupuy et al. (2017) found CH₄ photodesorption for monochromatic energies above 9.1 eV. However, in agreement with Cruz-Díaz et al. (2014) and Martín-Doménech et al. (2016), no evidence of a significant CH₄ photon-induced desorption was found in our work using the MDHL. Indeed, in our experiments, methane molecules are prone to dissociate rather than photodesorb. Recombination of radicals produce ethane and propane molecules, which were found to photochemidesorb. The excess energy released from the formation of photoproducts contributes to their desorption on the top monolayer. The constant ion current obtained for ethane and propane molecules during CH₄ ice irradiation supported the photochemidesorption mechanism, as explained in Sect. 3.3. Additionally, C₂H₂ was found to photodesorb, producing a difference in the ion current of $\frac{m}{z} = 25$, and 26, when compared to other fragments of the hydrocarbons detected.

ACKNOWLEDGEMENTS

The Spanish Ministry of Science, Innovation and Universities supported this research under grant number AYA2017-85322-R (AEI/FEDER, UE), PhD fellowship FPU17/03172 and MDM-2017-0737 Unidad de Excelencia "María de Maeztu"– Centro de Astrobiología (CSIC-INTA). G. A. Cruz-Díaz was supported by the National Aeronautics and Space Administration through the NASA Astrobiology Institute under Cooperative Agreement Notice NNH13ZDA017C issued through the Science Mission Directorate.

REFERENCES

- Abplanalp M. J., Jones B. M., Kaiser R. I., 2018, Physical Chemistry Chemical Physics (Incorporating Faraday Transactions), 20, 5435
- Andersson S., van Dishoeck E. F., 2008, A&A, 491, 907
- Baratta G. A., Leto G., Palumbo M. E., 2002, A&A, 384, 343
- Bennett C. J., Jamieson C. S., Osamura Y., Kaiser R. I., 2006, ApJ, 653, 792
- Bertin M., et al., 2016, ApJ, 817, L12

- Boogert A. C. A., et al., 1996, *A&A*, 315, L377
- Boogert A. C. A., Gerakines P. A., Whittet D. C. B., 2015, *ARA&A*, 53, 541
- Bossa J. B., Paardekooper D. M., Isokoski K., Linnartz H., 2015, *Physical Chemistry Chemical Physics (Incorporating Faraday Transactions)*, 17, 17346
- Cecchi-Pestellini C., Aiello S., 1992, *MNRAS*, 258, 125
- Cruikshank D. P., Roush T. L., Owen T. C., Geballe T. R., de Bergh C., Schmitt B., Brown R. H., Bartholomew M. J., 1993, *Science*, 261, 742
- Cruz-Díaz G. A., Muñoz Caro G. M., Chen Y. J., Yih T. S., 2014, *A&A*, 562, A120
- Cruz-Díaz G. A., Martín-Doménech R., Muñoz Caro G. M., Chen Y. J., 2016, *A&A*, 592, A68
- Dartois E., 2005, *Space Sci. Rev.*, 119, 293
- Dartois E., Muñoz Caro G. M., Deboffle D., Montagnac G., d'Hendecourt L., 2005, *A&A*, 432, 895
- Dupuy R., et al., 2017, *A&A*, 603, A61
- Fayolle E. C., et al., 2013, *A&A*, 556, A122
- Fillion J.-H., et al., 2014, *Faraday Discussions*, 168, 533
- Gerakines P. A., Schutte W. A., Ehrenfreund P., 1996, *A&A*, 312, 289
- González Díaz C., Carrascosa de Lucas H., Aparicio S., Muñoz Caro G. M., Sie N.-E., Hsiao L.-C., Cazaux S., Chen Y.-J., 2019, *MNRAS*, 486, 5519
- Gredel R., Lepp S., Dalgarno A., Herbst E., 1989, *ApJ*, 347, 289
- Grundy W. M., et al., 2016, *Science*, 351, aad9189
- Hudson R. L., Moore M. H., Raines L. L., 2009, *Icarus*, 203, 677
- Hudson R. L., Gerakines P. A., Loeffler M. J., 2015, *Physical Chemistry Chemical Physics (Incorporating Faraday Transactions)*, 17, 12545
- Kaiser R. I., Roessler K., 1998, *ApJ*, 503, 959
- Lacy J. H., Carr J. S., Evans Neal J. I., Baas F., Achtermann J. M., Arens J. F., 1991, *ApJ*, 376, 556
- Lin M.-Y., Lo J.-I., Lu H.-C., Chou S.-L., Peng Y.-C., Cheng B.-M., Ogilvie J. F., 2014, *The Journal of Physical Chemistry A*, 118, 3438
- Lo J.-I., Lin M.-Y., Peng Y.-C., Chou S.-L., Lu H.-C., Cheng B.-M., Ogilvie J. F., 2015, *MNRAS*, 451, 159
- Lu H.-C., Chen H.-K., Cheng B.-M., 2004, *Analytical chemistry*, 76, 5965
- Luna R., Luna-Ferrández R., Millán C., Domingo M., Muñoz Caro G. M., Santonja C., Satorre M. Á., 2017, *ApJ*, 842, 51
- Martín-Doménech R., Manzano-Santamaría J., Muñoz Caro G. M., Cruz-Díaz G. A., Chen Y. J., Herrero V. J., Tanarro I., 2015, *A&A*, 584, A14
- Martín-Doménech R., Muñoz Caro G. M., Cruz-Díaz G. A., 2016, *A&A*, 589, A107
- Martín-Doménech R., Cruz-Díaz G. A., Muñoz Caro G. M., 2018, *MNRAS*, 473, 2575
- McKay C. P., Martin S. C., Griffith C. A., Keller R. M., 1997, *Icarus*, 129, 498
- Moore M. H., Hudson R. L., 2003, *Icarus*, 161, 486
- Muñoz Caro G. M., Jiménez-Escobar A., Martín-Gago J. Á., Rogero C., Atienza C., Puertas S., Sobrado J. M., Torres-Redondo J., 2010, *A&A*, 522, A108
- Mumma M. J., Charnley S. B., 2011, *Annual Review of Astronomy and Astrophysics*, 49, 471
- Öberg K. I., Boogert A. C. A., Pontoppidan K. M., Blake G. A., Evans N. J., Lahuis F., van Dishoeck E. F., 2008, *ApJ*, 678, 1032
- Öberg K. I., van Dishoeck E. F., Linnartz H., Andersson S., 2010, *ApJ*, 718, 832
- Öberg K. I., Boogert A. C. A., Pontoppidan K. M., van den Broek S., van Dishoeck E. F., Bottinelli S., Blake G. A., Evans II N. J., 2011, *ApJ*, 740, 109
- Okabe H., 1978, *Photochemistry of small molecules*
- Owen T. C., et al., 1993, *Science*, 261, 745
- Shen C. J., Greenberg J. M., Schutte W. A., van Dishoeck E. F., 2004, *A&A*, 415, 203
- Wong M. L., et al., 2017, *Icarus*, 287, 110
- Wu Y.-J., Wu C. Y. R., Chou S.-L., Lin M.-Y., Lu H.-C., Lo J.-I., Cheng B.-M., 2012, *ApJ*, 746, 175
- Young L. A., et al., 2018, *Icarus*, 300, 174
- d'Hendecourt L. B., Allamandola L. J., Grim R. J. A., Greenberg J. M., 1986, *A&A*, 158, 119
- d'Hendecourt L., et al., 1996, *A&A*, 315, L365
- de Barros A. L. F., Bordalo V., Seperuelo Duarte E., da Silveira E. F., Domaracka A., Rothard H., Boduch P., 2011, *A&A*, 531, A160
- van Hemert M. C., Takahashi J., van Dishoeck E. F., 2015, *Journal of Physical Chemistry A*, 119, 6354

This paper has been typeset from a T_EX/L^AT_EX file prepared by the author.